Electron transport in nanoporous graphene: Probing the Talbot effect

Calogero, Gaetano; Papior, Nick Rübner; Kretz, Bernhard; Garcia-Lekue, Aran; Frederiksen, Thomas; Brandbyge, Mads

Published in:
Nano Letters

Link to article, DOI:
10.1021/acs.nanolett.8b04616

Publication date:
2019

Document Version
Peer reviewed version

Electron Transport in Nanoporous Graphene: Probing the Talbot Effect

Gaetano Calogero,[*,†] Nick R. Papior,[†] Bernhard Kretz,[‡] Aran Garcia-Lekue,[¶,§] Thomas Frederiksen,[¶,§] and Mads Brandbyge[*,†]

†*Dept. of Micro- and Nanotechnology, Technical University of Denmark, Center for Nanostructured Graphene (CNG), DK-2800 Kongens Lyngby, Denmark*

‡*Institute of Theoretical Physics, University of Regensburg, 93040 Regensburg, Germany*

¶*Donostia International Physics Center (DIPC), 20018 San Sebastian, Spain.*

§*Ikerbasque, Basque Foundation for Science, 48013 Bilbao, Spain.*

E-mail: gaca@nanotech.dtu.dk; mads.brandbyge@nanotech.dtu.dk

Phone: +4591198180; +4545256328

Abstract

Electrons in graphene can show diffraction and interference phenomena fully analogous to light thanks to their Dirac-like energy dispersion. However it is not clear how this optical analogy persists in nanostructured graphene, e.g. with pores. Nanoporous graphene (NPG) consisting of linked graphene nanoribbons has recently been fabricated using molecular precursors and bottom-up assembly [Moreno *et al*, *Science* **360**, 199 (2018)]. We predict that electrons propagating in NPG exhibit the interference Talbot effect, analogous to photons in coupled waveguides. Our results are obtained by parameter-free atomistic calculations of real-sized NPG samples, based on seamlessly integrated density functional theory and tight-binding regions. We link the origins of this interference phenomenon to the band structure of the NPG. Most importantly, we demonstrate how the Talbot effect may be detected experimentally using dual-probe scanning tunneling microscopy. Talbot interference of electron waves in NPG or other related materials may open up new opportunities for future quantum electronics, computing or sensing.

Keywords

Nanoporous graphene, Talbot interference, electron transport, scanning probe microscopy, multi-scale modeling

Controlling electron waves by harnessing phase-coherence and interference effects is a cornerstone for future nano-electronics,[1,2] quantum computing,[3] sensing[4] or electron beam splitting.[5] To this end, design of platforms with well-defined, narrow and low-loss propagation channels is essential.

Nanoporous graphene (NPG) holds great potential for distributing and controlling currents at the nanoscale.[6,7] By achieving bottom-up synthesis and transfer of atomically precise NPGs Moreno *et al.*[8] have recently paved the way for fabrication of high-quality NPG-based devices. Further functionalization or engineering of the pore edges could offer additional opportunities to manipulate electron transport.[9] The particular edge topology of the linked graphene nanoribbons (GNRs) making up the NPG results in a pronounced in-plane anisotropy, which is reflected in the electronic structure as a peculiar energy-dependent 1D localization of electron states near the conduction band. Two-terminal electrical measurements and simulations successfully proved the semiconducting nature of NPG and the anisotropic electron propagation within the mesh.[8] However, the fixed electrode setup did not answer the question of how transmitted electrons are confined in a single GNR and whether one-dimensional directed electron flow is possible. Moreover, it is unclear to what extend the typical optics analogy used for electron transport in pristine graphene devices[10–13] can work for devices based on NPG.

Visualizing current flow in NPG represents the most direct route to tackle these questions in an experiment. Several techniques based on superconducting interferometry,[14,15] scanning gate microscopy[16] or diamond-NV centers[17] have demonstrated how imaging real-space current flow in graphene structures can profitably underpin standard electrical measurements for classical or quantum transport phenomena, while scanning probe spectroscopies are now proving to be able to probe these currents at the atomic scale.[18]

In this letter we theoretically investigate to what extent one can inject currents along individual GNR channels in gated NPG-based devices contacted chemically to a scanning tunneling microscope (STM) probe. We develop a multi-scale method based on Density

Functional Theory (DFT) and Non-Equilibrium Green's functions (NEGF), enabling current calculations with devices longer than 100 nm, relevant for experiments. This is accomplished by linking a perturbed contact region described by DFT to an unperturbed large-scale region described by an effective tight-binding (TB) model parametrized from DFT. We find that the inter-GNR coupling disrupts the longitudinal electron confinement into individual channels, giving rise to the Talbot effect, a fascinating interference phenomenon predicted to occur in discrete optical wave-guide systems.[19–24] The fine detail of Talbot wave interference is the origin of various technological applications, ranging from lithography[25] to phase-contrast interferometry.[26] Besides, it was predicted to occur for massless Dirac Fermions in graphene[23] as well as plasmons in single-mode GNRs arrays.[24] We prove the robustness of the electronic Talbot effect in NPG by injecting current from the STM tip into various NPG sites and under various gating conditions. Using proof-of-principle calculations we also predict how this effect can be detected using a second STM tip.

We carry out transport calculations based on NEGF[27–29] applied to DFT or TB models, using TranSiesta,[30,31] TBtrans[31] and sisl.[32] While parameter-free DFT models limit the accessible device sizes to only a few nanometers, parameterized TB can capture basic transport features of large systems with minor chemical perturbations (e.g. metal contact or chemical hybridization). The DFT model for the NPG device, shown in Fig. 1a, covers an area of $6.5 \times 5.5\,\mathrm{nm}^2$ (1449 atoms) and it is defined on a single-ζ polarized basis set. This choice guarantees enough accuracy over an energy range of $\sim \pm 2\,\mathrm{eV}$ from E_F. A better basis would be needed to capture superatom bands at $E - E_\mathrm{F} > 2\,\mathrm{eV}$.[8,33] We use the GGA-PBE exchange-correlation functional[34] and open (periodic) boundary conditions along y (x), while sampling the x direction with 5 k-points. Pores are passivated with H atoms and a model Au tip is in chemical contact with the NPG. The tip structure is chosen so as to ensure a flat local density of states on the tip apex over the range $[-0.75\,\mathrm{eV}, 1\,\mathrm{eV}]$, relevant for our study. The coordinates of the tip apex and up to 20 C atoms nearby are optimized until forces are less than $0.01\,\mathrm{eV/\AA}$. After the optimization the Au-C bond-length is $\sim 2.0\,\mathrm{\AA}$. In order

to describe a more realistic experimental environment we self-consistently include a bottom gate in the calculations. This is done by fixing spatial charge in a *gate-layer* placed 15 Å beneath the NPG, so as to dope it by $n_g = \pm 10^{13}\, e^- \mathrm{cm}^{-2}$.[35] The device Green's function is calculated as

$$\mathbf{G} = \left[\mathbf{S}\,(E + i\eta) - \mathbf{H} - \sum_i \mathbf{\Sigma}_i \right]^{-1} \tag{1}$$

where $\mathbf{S}$ and $\mathbf{H}$ are the model overlap and Hamiltonian and $\mathbf{\Sigma}_i$, called *self-energies*, connect the device to semi-infinite regions along x (electrodes). A self-energy allows to seamlessly connect different regions, be it infinite bulk or localized perturbations. We exploit this to embed one or more DFT-precision regions inside much larger TB models, needed to reach experimental relevant dimensions and observe interference. The central idea of this multi-scale approach is to construct the self-energy connecting p_z orbitals of the outermost unperturbed DFT atoms (shaded frame in Fig. 1a) to a larger p_z TB model. We obtain TB parameters from a DFT calculation of unperturbed NPG, such that the resulting model retains the interaction range of the DFT basis set, is non-orthogonal and takes self-consistent effects of gates and/or bias into account. Therefore, besides introducing local DFT-precision in the TB model, this method enables TB-based N-electrode transport calculations without any fitting parameters. See Supporting Information for details on the DFT calculations and the multi-scale method.

We consider two different positions of the tip, namely on top of a C atom in the middle of a ribbon or at a bridge between two C atoms linking two ribbons (see inset to Fig. 1a). In the former case the C atoms below the tip are pushed ~ 0.3 Å below the NPG plane, while at the bridge site the tip binds to two aromatic rings causing a slight torsion.

The main effect of gating on the NPG electronic structure is a rigid band shift of ± 0.35 eV for n- and p-type doping cases, respectively (Fig. 1b). We find in both cases a band gap of ~ 0.7 eV between symmetric valence and conduction bands, in good agreement with results obtained for non-gated NPG.[8] Bands with predominant longitudinal character are clearly visible at energies up to $0.7 - 0.8$ eV above (below) the conduction (valence) band (shaded

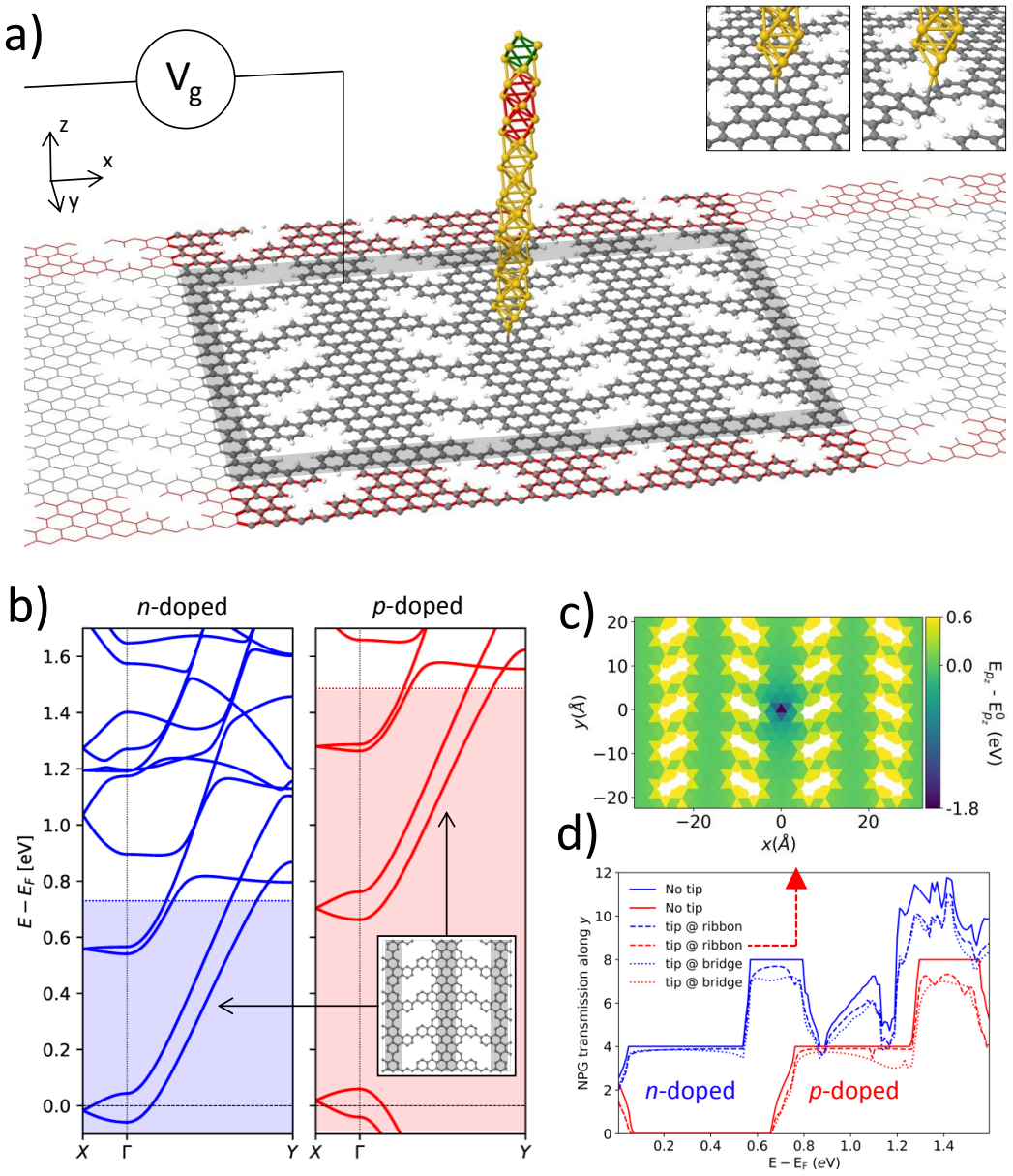

Figure 1: **DFT model of NPG.** (a) DFT model of gated NPG-based device with contact to STM tip. Electrodes are highlighted in red. Insets show the optimized contact regions for ribbon and bridge positions. The shaded area delimits the device region. (b) Band structure of the NPG unit cell in two gated conditions inducing either n-type (blue, $n_g = +10^{13}\,e^-\mathrm{cm}^{-2}$) or p-type (red, $n_g = -10^{13}\,e^-\mathrm{cm}^{-2}$) doping. States with energies in the shaded areas, i.e. up to $\sim 0.7\,\mathrm{eV}$ above (below) the conduction (valence) band, disperse more along $\Gamma - Y$ than along $\Gamma - X$, hence defining predominantly longitudinal transport channels. (c) On-site potential of C p_z orbitals in a p-doped NPG. Values are relative to the average potential $E^0_{p_z}$ in the bulk of ribbons $\sim 0.5\,\mathrm{nm}$ away from the tip. Beyond this distance the perturbation from the tip is effectively screened. (d) Transmission between the two NPG electrodes, with and without tip contact, for the two different tip positions in (a) and gated conditions in (b).

areas), where states along $\Gamma - Y$ indeed disperse more than those along $\Gamma - X$. The contact with the tip causes local variation of the C p_z potential which is screened at $\sim 0.5\,\mathrm{nm}$ from the tip (Fig. 1c). This degrades transmission between the two NPG electrodes along the y direction (Fig. 1d). For all energies in the longitudinal regime transport is essentially one-dimensional along the GNRs, due to the weak inter-ribbon coupling. The onset at $E \sim 0.9\,\mathrm{eV}$ of bands with dominant transverse character disrupts the 1D confinement and conductance quantization is lost.

For both n- and p-type NPG and both tip positions we find qualitatively similar electronic and transport features (see Supporting Information, Figs. S1, S2). Therefore, without loss of generality, we focus in the following on the n-doped NPG case probed at the ribbon site.

We visualize the electron flow near the contact through the injected density of states[1] and bond-currents from the tip,[2] as shown in Fig. 2a-b. These clearly demonstrate electron confinement inside the probed ribbon up to distances comparable to the DFT cell size, for all energies ranging from the conduction band up to $\sim 0.7\,\mathrm{eV}$ above it (see Supporting Information, Fig. S2). We study the distribution of electronic current in the far-field, i.e. far from the source by performing transport calculations where the DFT "injection region" is embedded into a larger TB NPG model. We benchmark the applicability of this method by embedding the DFT-precision injection region in a TB-region which has the same boundary conditions and size of the DFT transport setup (see Supporting Information, Fig. S4). The results show that we can reproduce the DFT transmission spectra in the longitudinal regime (Fig. 1b, shaded) by the combined DFT+TB model.

Next we embed the DFT injection region as electrode in a large $100\,\mathrm{nm} \times 120\,\mathrm{nm}$ TB model of a device with two NPG electrodes along y and a complex absorbing potential[37,38] along x. This larger model reveals that at distances beyond the DFT cell size transversal losses

[1] Injected density of states is calculated by summing the absolute modules of the three eigenchannels[36] which contribute the most to transmission from the tip to the NPG electrodes.

[2] Bond-currents are defined as $J_{\alpha\beta} = \sum_{\nu\in\alpha}\sum_{\mu\in\beta} J_{\nu\mu}$, where ν (μ) indicates a basis orbital centered on atom α (β).

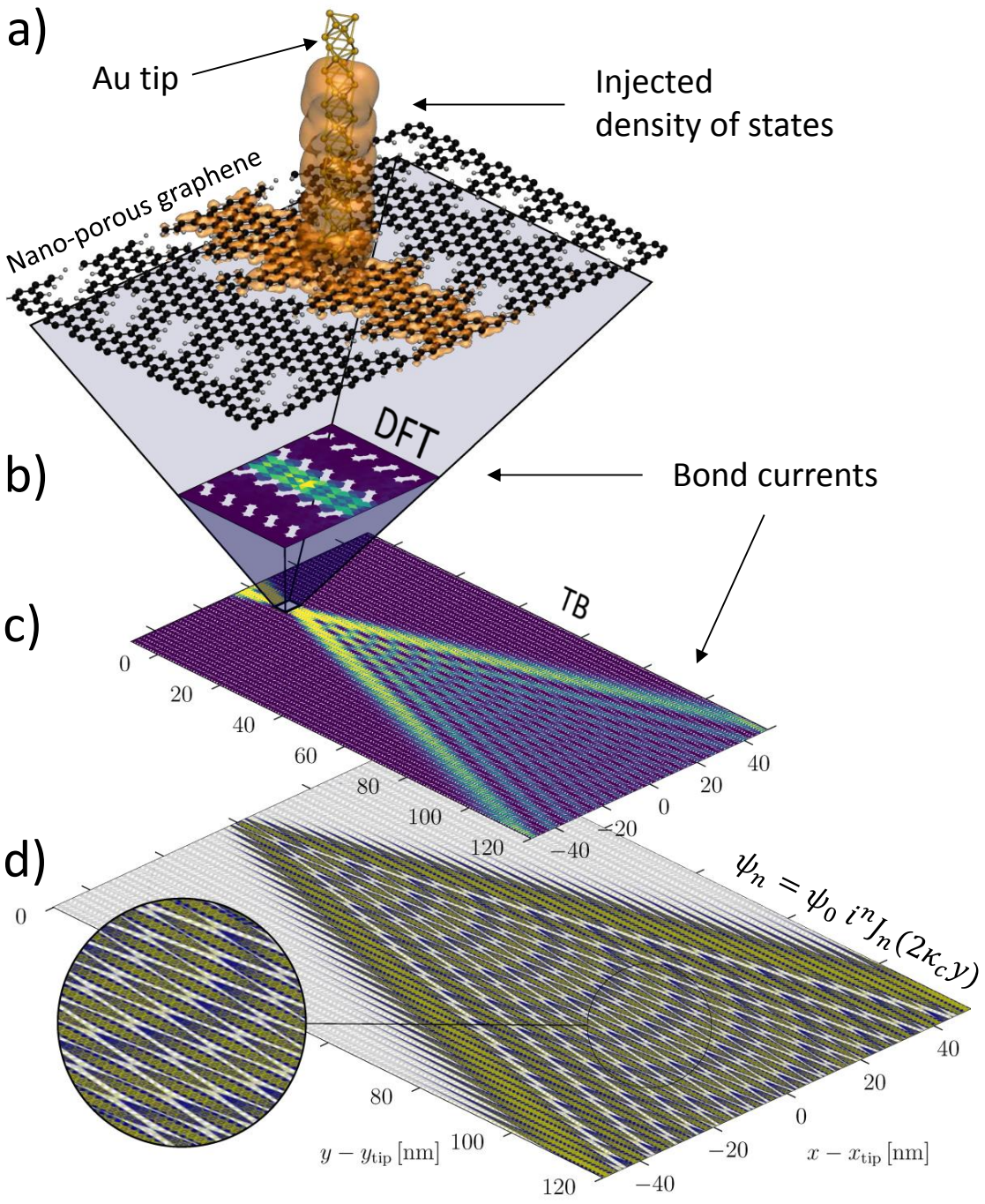

Figure 2: **Talbot effect from multi-scale calculations for n-doped NPG.** The figure shows (a) DFT geometry and density of states injected by the tip, (b) bond-currents at $E - E_{\text{F}} = 0.2\,\text{eV}$ obtained with the DFT model and (c) a large-scale TB model with DFT-precision injection, and (d) the best-fit to the Talbot effect equations. In (d) the local spectral density of states (ADOS) from the tip is shown in yellow, scaled by $y - y_{\text{tip}}$ to compensate damping occurring far from the tip. The fitted equations ψ_n are plotted in blue underneath the ADOS. The integers $n \in [-26, 26]$ index the 53 GNR rows along the y-direction (covering a width of 100 nm across the x-axis).

significantly affect the far-field behavior (Fig. 2c). Current splits into neighboring ribbons with a certain periodicity of $\sim 7-8\,\mathrm{nm}$. The resulting "beams" diverge from the y direction with a maximum angle which varies slightly with energy (see Supporting Information, Fig. S5). In particular when the tip injects into a ribbon site this angle decreases from $\sim 30°$ for $E - E_\mathrm{F} < 0.3\,\mathrm{eV}$ to $\sim 20°$ for $0.4\,\mathrm{eV} < E - E_\mathrm{F} < 0.8\,\mathrm{eV}$. We observe similar results for injection into a bridge site, although the interference in this case is more blurred, since the injected currents start out by propagation in the two bridged ribbons (see Supporting Information, Fig. S2). We also find that application of a finite bias voltage between the tip and the NPG does not disrupt the interference pattern (see Supporting Information, Fig. S6).

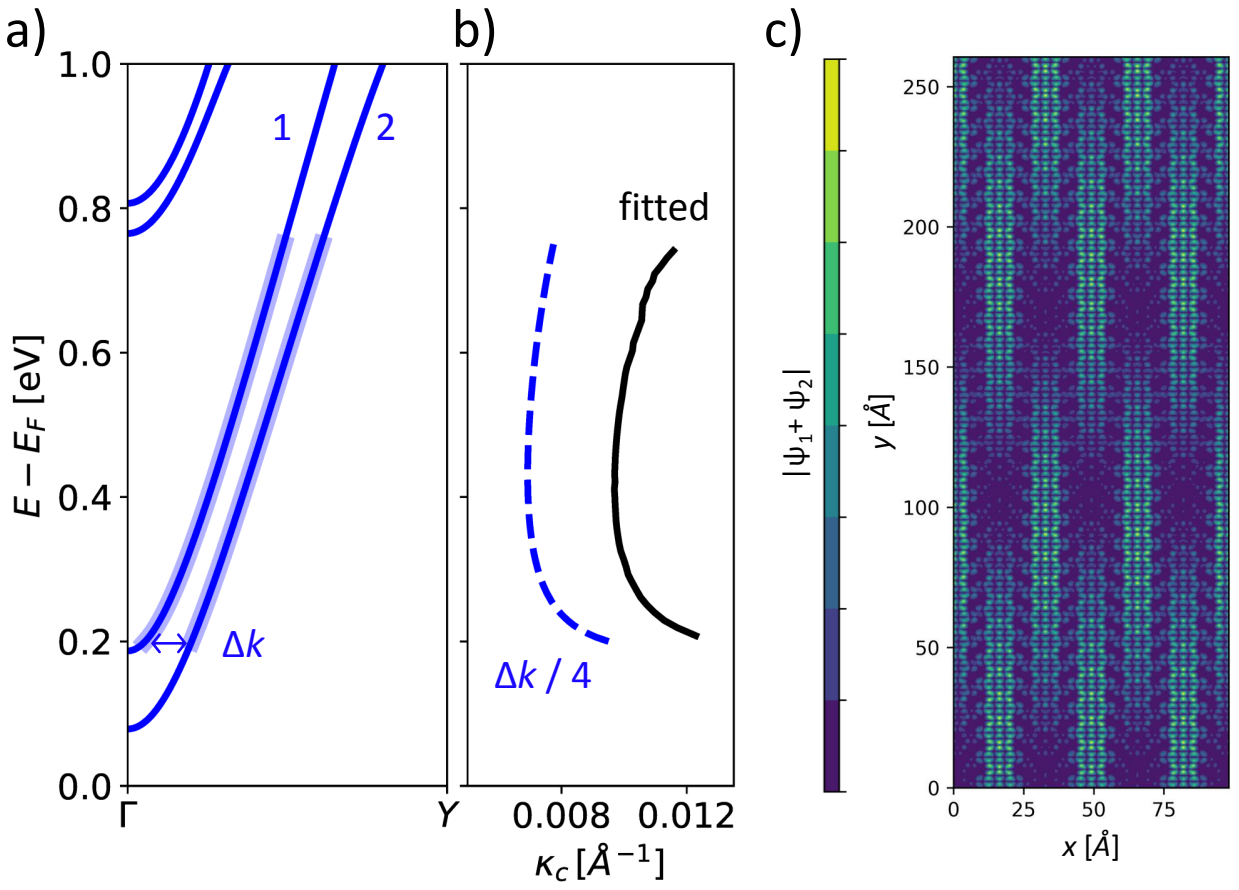

Figure 3: **Origin of Talbot effect.** (a) Longitudinal bands for a p_z TB model of n-doped NPG parameterized from DFT. (b) Energy dependence of inter-GNR coupling κ_c from fit to the Talbot equations Eq. (3), in comparison to $\Delta k/4 = |k_2 - k_1|/4$. (c) Amplitude of $\psi_1 + \psi_2$ at $E - E_\mathrm{F} = 0.2\,\mathrm{eV}$, showing the interference underlying the Talbot effect.

The Talbot interference generally refers to repeated self-imaging of a diffraction grating.[20] In this context the wave amplitude ψ_n inside the n^{th} element of an infinite array of weakly coupled discrete channels aligned along y obeys the following discrete differential equation[21,39–41]

$$i\,\frac{d\psi_n}{dy}(y) + \kappa_c\,[\psi_{n-1}(y) + \psi_{n+1}(y)] = 0, \tag{2}$$

where κ_c represents the inter-channel coupling coefficient. The coefficient κ_c can be regarded as a figure-of-merit for the degree of 1D confinement in the elements of the array: the lower the value of κ_c, the lower the spread into the weakly coupled adjacent channels. In the particular case when only a single channel is initially excited, i.e. $\psi_{n=0} = \psi_0$, the solutions for Eq. (2) can be written as[24,39,41]

$$\psi_n(y) = \psi_0\, i^n\, J_n(2\kappa_c y), \tag{3}$$

where J_n is the Bessel function of the n^{th} order.

We find that the square modulus of Eq. (3) can be fitted to the far-field spectral density of states originating from the tip. The best fit on a set of 53-channels of a $100\,\text{nm} \times 120\,\text{nm}$ n-doped NPG is illustrated in Fig. 2d. The fitted values at $E = 0.2\,\text{eV}$ are $\psi_0 = 0.037$ and $\kappa_c = 0.012\,\text{Å}^{-1}$. The latter varies slightly with energy as shown in Fig. 3b.

The Talbot effect originates due to interference of the two longitudinal Bloch states ψ_1 and ψ_2. From the momentum difference one can estimate the coupling strength as $\kappa_c = \Delta k/4 = |k_2 - k_1|/4$.[23,24] In Fig. 3c we plot $|\psi_1 + \psi_2|$ for the NPG without tip contact, showing the regular interference pattern expected when all GNRs are simultaneously excited.[23]

The latest developments in STM have enabled measurements with up to four tips[42] and control over tip-tip distance down to tens of nm.[18] Within this context, we propose to use dual-probe STM to reveal the electronic Talbot effect experimentally. One probe can be used to inject current into the NPG at a fixed position as discussed above while the second probe is used to map out the interference pattern. The tips are in chemical contact with

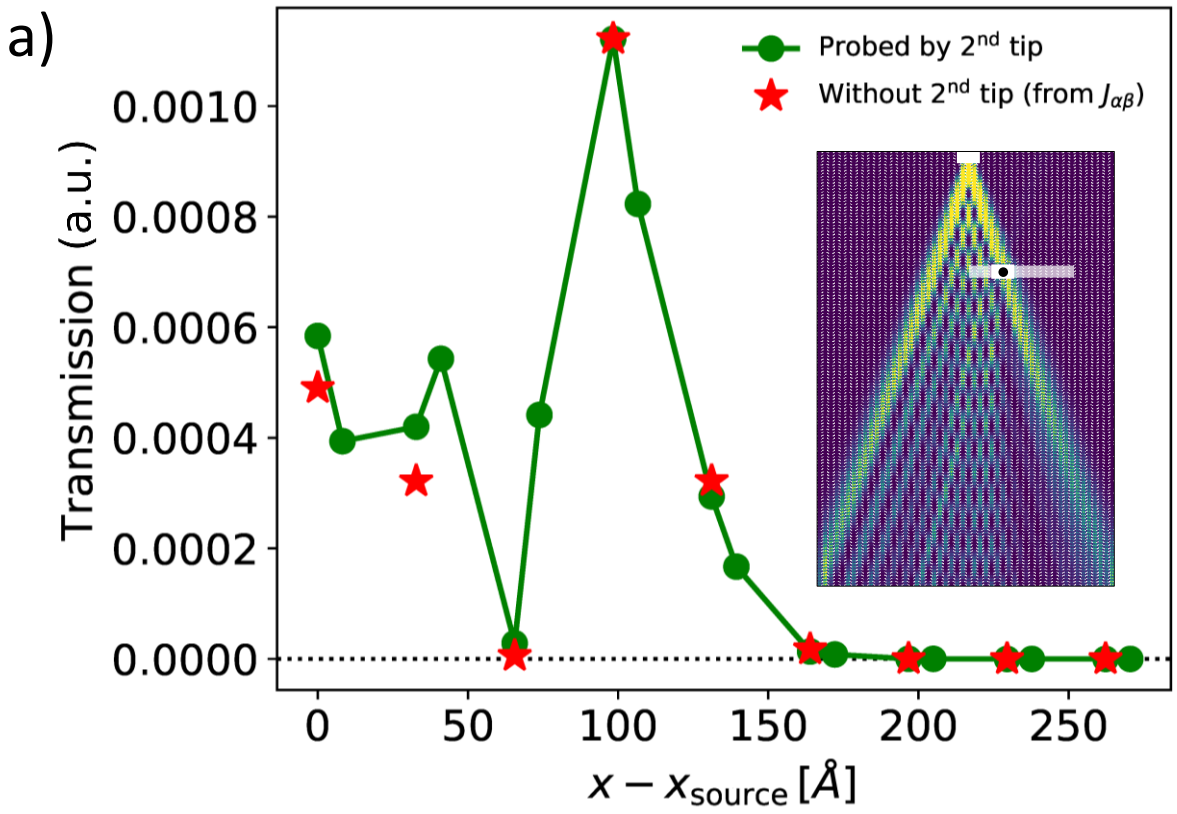

Figure 4: **Probing the Talbot effect.** (a) Transmission at $E - E_{\mathrm{F}} = 0.2\,\mathrm{eV}$ (green) measured by a 2nd DFT-precision tip probing ribbon and bridge sites of n-doped NPG along the white line shown in inset, in comparison with bond-currents flowing in absence of the 2nd tip (red). These are obtained on a "per ribbon" basis by summing all bond-currents passing through the white line, without distinction between ribbon and bridge sites, and then scaling by a factor 1/16. The inset shows bond-currents injected into the NPG (with same size as in Fig. 2c) and scattering off the 2nd tip for one of the scanned positions, indicated by the black dot.

the NPG rather than tunnel contacts in order to maximize the current, important for the experimental feasibility. We use the modular capability of the multi-scale approach to embed two DFT-precision tips in the large TB model. Both tips are located $\sim 2\,\text{Å}$ above NPG and we fix the probe-tip distance to around 30 nm from the source. The probe-tip is moved between the bridge and ribbon positions along the white line shown in the inset in Fig. 4a. The calculated transmission between the two tips, injecting electrons at $E - E_{\text{F}} = 0.2\,\text{eV}$ into n-doped NPG, is shown in Fig. 4a. The maxima of transmission reproduce the maxima of bond-currents injected from the source in absence of the second tip within 5%. This proves that the signal in electric current detected by the second tip can map out the Talbot interference pattern. This also indicates that modifications of the NPG atomic structure and electron density due to the chemical contact with the tip do not suppress the effect. That being said, we speculate that evidence for the Talbot effect in NPG may be obtained by devising other types of experiments.

In conclusion, we have explored how electrons injected by a STM probe in chemical contact to gated NPG-based devices behave in near and far field. By performing multi-scale parameter-free calculations of large-scale TB models of NPG with DFT-precision regions we found a clear signature of phase-coherent electron waves, manifested in the far field as a Talbot interference effect. The origin of this phenomenon is the cross-talk between longitudinal 1D channels (GNRs) making up the NPG. Using proof-of-principle multi-probe calculations we have shown this interference effect may be observed in a dual-probe STM experiment.

Further investigations could potentially shed light on the important impact of defects, substrate or pore functionalization on the current flow. Importantly, chemical design of the inter-ribbon bridges could allow fine-tuning of the coupling strength κ_c to improve 1D transport confinement. We also speculate that the Talbot effect could be observed in other structures featuring weakly coupled quasi-1D channels, such as other anisotropic 2D materials[43–47] or crystals hosting surface states.[48] This effect in elastic, phase-coherent transport

may be used to gain insights into the phase-breaking length in these structures due to various scattering mechanisms such as electron-phonon coupling. Finally, since topologically non-trivial states were found at the edges of chiral GNRs,[49,50] further studies may potentially reveal whether topological signatures could emerge in NPGs.

Acknowledgement

Financial support by Villum Fonden (00013340), Danish research council (4184-00030), Spanish Ministerio de Economía y Competitividad (FIS2017-83780-P and MAT2016-78293-C6-4-R), UPV/EHU (IT-756-13) is gratefully acknowledged. The Center for Nanostructured Graphene (CNG) is sponsored by the Danish Research Foundation (DNRF103). We are thankful to Sidsel R. Papior, José Caridad, Pedro Brandimarte, Isaac Alcón Rovira and Stephen Power for useful discussions.

Supporting Information Available

Computational details, DFT potential and charge distributions in gated NPG+tip systems, transmission and near-field bond-currents from tip to DFT-modeled NPG, multiscale method applied to NPG+tip systems, transmission and far-field bond-currents from DFT-precision tip to TB-modeled NPG, bond-current maps from dual-probe calculations.

References

(1) Chen, L.; Zhang, Y.; Chen, G.; Franco, I. Stark control of electrons along nanojunctions. *Nat. Commun.* **2018**, *9*, 2070.

(2) Biele, R.; Rodríguez-Rosario, C. A.; Frauenheim, T.; Rubio, A. Controlling heat and particle currents in nanodevices by quantum observation. *npj Quantum Mater.* **2017**, *2*, 38.

(3) Karra, M.; Sharma, K.; Friedrich, B.; Kais, S.; Herschbach, D. Prospects for quantum computing with an array of ultracold polar paramagnetic molecules. *J. Chem. Phys.* **2016**, *144*, 094301.

(4) Prindle, A.; Samayoa, P.; Razinkov, I.; Danino, T.; Tsimring, L. S.; Hasty, J. A sensing array of radically coupled genetic 'biopixels'. *Nature* **2011**, *481*, 39.

(5) Brandimarte, P.; Engelund, M.; Papior, N.; Garcia-Lekue, A.; Frederiksen, T.; Sánchez-Portal, D. A tunable electronic beam splitter realized with crossed graphene nanoribbons. *J. Chem. Phys.* **2017**, *146*, 092318.

(6) Pedersen, T. G.; Flindt, C.; Pedersen, J.; Mortensen, N. A.; Jauho, A.-P.; Pedersen, K. Graphene Antidot Lattices: Designed Defects and Spin Qubits. *Phys. Rev. Lett.* **2008**, *100*, 136804.

(7) Bai, J.; Zhong, X.; Jiang, S.; Huang, Y.; Duan, X. Graphene nanomesh. *Nat. Nanotechnol.* **2010**, *5*, 190.

(8) Moreno, C.; Vilas-Varela, M.; Kretz, B.; Garcia-Lekue, A.; Costache, M. V.; Paradinas, M.; Panighel, M.; Ceballos, G.; Valenzuela, S. O.; Peña, D.; Mugarza, A. Bottom-up synthesis of multifunctional nanoporous graphene. *Science* **2018**, *360*, 199–203.

(9) Caridad, J. M.; Calogero, G.; Pedrinazzi, P.; Santos, J. E.; Impellizzeri, A.; Gunst, T.; Booth, T. J.; Sordan, R.; Bøggild, P.; Brandbyge, M. A Graphene-Edge Ferroelectric Molecular Switch. *Nano Lett.* **2018**, *18*, 4675–4683.

(10) Chen, S.; Han, Z.; Elahi, M. M.; Habib, K. M. M.; Wang, L.; Wen, B.; Gao, Y.; Taniguchi, T.; Watanabe, K.; Hone, J.; Ghosh, A. W.; Dean, C. R. Electron optics with p-n junctions in ballistic graphene. *Science* **2016**, *353*, 1522–1525.

(11) Caridad, J. M.; Connaughton, S.; Ott, C.; Weber, H. B.; Krstić, V. An electrical analogy to Mie scattering. *Nat. Commun.* **2016**, *7*, 12894.

(12) Bøggild, P.; Caridad, J. M.; Stampfer, C.; Calogero, G.; Papior, N. R.; Brandbyge, M. A two-dimensional Dirac fermion microscope. *Nat. Commun.* **2017**, *8*.

(13) Xu, H. Y.; Wang, G. L.; Huang, L.; Lai, Y. C. Chaos in Dirac Electron Optics: Emergence of a Relativistic Quantum Chimera. *Phys. Rev. Lett.* **2018**, *120*, 124101.

(14) Allen, M. T.; Shtanko, O.; Fulga, I. C.; Akhmerov, A. R.; Watanabe, K.; Taniguchi, T.; Jarillo-Herrero, P.; Levitov, L. S.; Yacoby, A. Spatially resolved edge currents and guided-wave electronic states in graphene. *Nat. Phys.* **2015**, *12*, 128.

(15) Silveiro, I.; Ortega, J. M. P.; de Abajo, F. J. G. Quantum nonlocal effects in individual and interacting graphene nanoribbons. *Light: Sci. Appl.* **2015**, *4*, e241.

(16) Bhandari, S.; Lee, G.-H.; Klales, A.; Watanabe, K.; Taniguchi, T.; Heller, E.; Kim, P.; Westervelt, R. M. Imaging Cyclotron Orbits of Electrons in Graphene. *Nano Lett.* **2016**, *16*, 1690–1694.

(17) Tetienne, J. P.; Dontschuk, N.; Broadway, D. A.; Stacey, A.; Simpson, D. A.; Hollenberg, L. C. Quantum imaging of current flow in graphene. *Sci. Adv.* **2017**, *3*, e1602429.

(18) Kolmer, M.; Olszowski, P.; Zuzak, R.; Godlewski, S.; Joachim, C.; Szymonski, M. Two-probe STM experiments at the atomic level. *J. Phys.: Condens. Matter* **2017**, *29*, 444004.

(19) Talbot Esq. F.R.S., H. F. LXXVI. Facts relating to optical science. no. IV. *Philos. Mag. (1798-1977)* **1836**, *9*, 401.

(20) Berry, M.; Marzoli, I.; Schleich, W. Quantum carpets, carpets of light. *Phys. World* **2001**, *14*, 39–44.

(21) Iwanow, R.; May-Arrioja, D. A.; Christodoulides, D. N.; Stegeman, G. I.; Min, Y.; Sohler, W. Discrete talbot effect in waveguide arrays. *Phys. Rev. Lett.* **2005**, *95*, 053902.

(22) Chen, Z.; Zhang, Y.; Xiao, M. Discrete Talbot effect in two-dimensional waveguide arrays. *Opt. Express* **2015**, *23*, 14724.

(23) Walls, J. D.; Hadad, D. The talbot effect for two-dimensional massless Dirac fermions. *Sci. Rep.* **2016**, *6*, 1–11.

(24) Wang, L.; Jia, Y.; Ji, Z. Discrete plasmonic Talbot effect in single-mode graphene ribbon arrays. *Appl. Opt.* **2017**, *56*, 9998–10002.

(25) Solak, H.; Dais, C.; Clube, F. Displacement Talbot lithography: a new method for high-resolution patterning of large areas. *Opt. Express* **2011**, *19*, 10686–10691.

(26) Birnbacher, L.; Willner, M.; Velroyen, A.; Marschner, M.; Hipp, A.; Meiser, J.; Koch, F.; Schröter, T.; Kunka, D.; Mohr, J.; Pfeiffer, F.; Herzen, J. Experimental Realisation of High-sensitivity Laboratory X-ray Grating-based Phase-contrast Computed Tomography. *Sci. Rep.* **2016**, *6*, 24022.

(27) Brandbyge, M.; Mozos, J.-L.; Ordejón, P.; Taylor, J.; Stokbro, K. Density-functional method for nonequilibrium electron transport. *Phys. Rev. B* **2002**, *65*, 165401.

(28) Datta, S. Nanoscale device modeling: the Green's function method. *Superlattices Microstruct.* **2000**, *28*, 253–278.

(29) Saha, K. K.; Nikolić, B. K.; Meunier, V.; Lu, W.; Bernholc, J. Quantum-Interference-Controlled Three-Terminal Molecular Transistors Based on a Single Ring-Shaped Molecule Connected to Graphene Nanoribbon Electrodes. *Phys. Rev. Lett.* **2010**, *105*, 236803.

(30) Soler, J. M.; Artacho, E.; Gale, J. D.; García, A.; Junquera, J.; Ordejón, P.; Sánchez-Portal, D. The SIESTA method for ab initio order-N materials simulation. *J. Phys.: Condens. Matter* **2002**, *14*, 2745–2779.

(31) Papior, N.; Lorente, N.; Frederiksen, T.; García, A.; Brandbyge, M. Improvements on non-equilibrium and transport Green function techniques: The next-generation transiesta. *Comput. Phys. Commun.* **2017**, *212*, 8–24.

(32) Papior, N. R. sisl: v0.9.5. 2018; `https://github.com/zerothi/sisl`.

(33) Papior, N. R.; Calogero, G.; Brandbyge, M. Simple and efficient LCAO basis sets for the diffuse states in carbon nanostructures. *J. Phys.: Condens. Matter* **2018**, *30*, 25LT01.

(34) Perdew, J. P.; Burke, K.; Ernzerhof, M. Generalized Gradient Approximation Made Simple. *Phys. Rev. Lett.* **1996**, *77*, 3865–3868.

(35) Papior, N.; Gunst, T.; Stradi, D.; Brandbyge, M. Manipulating the voltage drop in graphene nanojunctions using a gate potential. *Phys. Chem. Chem. Phys.* **2015**, *18*.

(36) Paulsson, M.; Brandbyge, M. Transmission eigenchannels from nonequilibrium Green's functions. *Phys. Rev. B* **2007**, *76*, 115117.

(37) Calogero, G.; Papior, R. N.; Bøggild, P.; Brandyge, M. Large-scale tight-binding simulations of quantum transport in ballistic graphene. *J. Phys.: Condens. Matter* **2018**, *30*, 364001.

(38) Xie, H.; Kwok, Y.; Jiang, F.; Zheng, X.; Chen, G. Complex absorbing potential based Lorentzian fitting scheme and time dependent quantum transport. *J. Chem. Phys.* **2014**, *141*, 164122.

(39) Yariv, A.; Yeh, P. *Optical Waves in Crystals. Propagation and Control of Laser Radiation.*; Wiley Series in Pure and Applied Optics, New York, 1984.

(40) Pertsch, T.; Zentgraf, T.; Peschel, U.; Bräuer, A.; Lederer, F. Anomalous refraction and diffraction in discrete optical systems. *Phys. Rev. Lett.* **2002**, *88*, 093901.

(41) Somekh, S.; Garmire, E.; Yariv, A.; Garvin, H. L.; Hunsperger, R. G. Channel optical waveguide directional couplers. *Appl. Phys. Lett.* **1973**, *22*, 46–47.

(42) Baringhaus, J.; Settnes, M.; Aprojanz, J.; Power, S. R.; Jauho, A. P.; Tegenkamp, C. Electron Interference in Ballistic Graphene Nanoconstrictions. *Phys. Rev. Lett.* **2016**, *116*, 186602.

(43) Lv, Y.; Chang, S.; Huang, Q.; Wang, H.; He, J. Scaling effect of phosphorene nanoribbon - Uncovering the origin of asymmetric current transport. *Sci. Rep.* **2016**, *6*, 38009.

(44) Kou, L.; Frauenheim, T.; Chen, C. Phosphorene as a Superior Gas Sensor: Selective Adsorption and Distinct I-V Response. *J. Phys. Chem. Lett.* **2014**, *5*, 2675–2681.

(45) Xia, F.; Wang, H.; Jia, Y. Rediscovering black phosphorus as an anisotropic layered material for optoelectronics and electronics. *Nat. Commun.* **2014**, *5*.

(46) Mannix, A. J.; Zhou, X.-F.; Kiraly, B.; Wood, J. D.; Alducin, D.; Myers, B. D.; Liu, X.; Fisher, B. L.; Santiago, U.; Guest, J. R.; Yacaman, M. J.; Ponce, A.; Oganov, A. R.; Hersam, M. C.; Guisinger, N. P. Synthesis of borophenes: Anisotropic, two-dimensional boron polymorphs. *Science* **2015**, *350*, 1513–1516.

(47) An, Y.; Jiao, J.; Hou, Y.; Wang, H.; Wu, D.; Wang, T.; Fu, Z.; Xu, G.; Wu, R. How does the electric current propagate through fully-hydrogenated borophene? *Phys. Chem. Chem. Phys.* **2018**, *20*, 21552–21556.

(48) Engelund, M.; Papior, N.; Brandimarte, P.; Frederiksen, T.; Garcia-Lekue, A.; Sánchez-Portal, D. Search for a Metallic Dangling-Bond Wire on n-Doped H-Passivated Semiconductor Surfaces. *J. Phys. Chem. C* **2016**, *120*, 20303–20309.

(49) Gröning, O.; Wang, S.; Yao, X.; Pignedoli, C. A.; Barin, G. B.; Daniels, C.; Cupo, A.; Meunier, V.; Feng, X.; Narita, A.; Müllen, K.; Ruffieux, P.; Fasel, R. Engineering of robust topological quantum phases in graphene nanoribbons. *Nature* **2018**, *560*, 209–213.

(50) Rizzo, D. J.; Veber, G.; Cao, T.; Bronner, C.; Chen, T.; Zhao, F.; Rodriguez, H.; Crommie, S. G. L. M. F.; Fischer, F. R. Topological Band Engineering of Graphene Nanoribbons. *Nature* **2018**, *560*, 204–208.

Graphical TOC Entry